Geosci. Model Dev. Discuss., doi:10.5194/gmd-2016-159, 2016
Manuscript under review for journal Geosci. Model Dev.
Published: 6 July 2016

Geoscientific Model Development Discussions
Open Access
EGU

Introducing UCLALES-SALSA: a large-eddy model with interactive sectional microphysics for aerosols, clouds and drizzle

Juha Tonttila[1], Zubair Maalick[3], Tomi Raatikainen[2], Harri Kokkola[1], Thomas Kühn[3], and Sami Romakkaniemi[1]

[1]Finnish Meteorological Institute, Atmospheric Research Centre of Eastern Finland, P.O. Box 1627, 70211 Kuopio, Finland
[2]Finnish Meteorological Institute, P.O. Box 503, 00101 Helsinki, Finland
[3]Department of Applied Physics, University of Eastern Finland, P.O. Box 1627, 70211 Kuopio, Finland

Correspondence to: Juha Tonttila (juha.tonttila@fmi.fi)

Abstract. Aerosol-cloud interactions and their impacts of global climate highlight the need for improved knowledge of the underlying physical processes and feedbacks as well as their interactions with cloud and boundary-layer dynamics. To pursue this goal, more sophisticated cloud-scale models are needed to complement the limited supply of observations. For this purpose, a new large-eddy simulation model, coupled with an interactive sectional description for aerosols and clouds, is introduced. The model, UCLALES-SALSA, builds and extends upon a well characterized LES model and microphysical model components. Novel strategies for the aerosol, cloud and drizzle bin layouts are presented. These enable tracking the effects of cloud processing and wet scavenging on the aerosol size distribution as accurately as possible while keeping the computational cost of the model acceptable. The model is tested with two different cases: one comprising a case with marine stratocumulus and another focusing on the formation and evolution of a nocturnal radiation fog. It is shown that the size-resolved interactions between aerosols and clouds have a critical influence on the dynamics of the boundary layer in both cases. The results demonstrate the importance of accurately representing the wet scavenging of aerosols in the model. Specifically, in a case with marine stratocumulus, drizzle formation and the subsequent removal of cloud activating particles lead to thinning of the cloud deck and the formation of a decoupled boundary layer structure. In radiation fogs the growth and sedimentation of droplets strongly affects their radiative properties, which in turn drive new droplet formation. The size resolved diagnostics provided by the model enable investigations of these issues with high detail. It is also shown that the results remain consistent with an earlier version of the UCLALES model in cases, where the dominating physical processes remain well represented by both.

1 Introduction

Large eddy simulators (LES) have been used to study the properties of clouds and the boundary layer for a few decades (e.g. Moeng, 1984). These models solve the low-pass filtered Navier-Stokes equations, i.e. the large energy-containing turbulent eddies are resolved, while the smallest length scales and energy dissipation are parameterized typically using closures based on the Smagorinsky model. This approach provides an attractive compromise between accuracy and computational burden, which is why LES models have become popular in studies of the properties of boundary-layers and clouds.

Geosci. Model Dev. Discuss., doi:10.5194/gmd-2016-159, 2016
Manuscript under review for journal Geosci. Model Dev.
Published: 6 July 2016

Geoscientific Model Development Discussions
Open Access
EGU

The typical grid resolution used in LES models ($\mathcal{O}$ tens of meters) enables a detailed representation of cloud structure and dynamics. However, the treatment of cloud microphysics is subject to high variability in terms of the level of detail and computational burden (Khain et al., 2015). The types of microphysical schemes and their implementation to LES models range from simple one or two moment bulk schemes, where droplet mass is predicted typically through saturation adjustment, with either prescribed or varying droplet number concentrations (Khairoutdinov and Kogan, 2000; Golaz et al., 2005; Seifert and Beheng, 2001, 2006; Stevens et al., 2005; Savre et al., 2014), to more elaborate ones with modal or sectional representations for the droplet size distributions (Feingold and Kreidenweis, 2002; Saleeby et al., 2015). In addition, there has been an increasing trend towards including representations for aerosol particles in these models as well (Feingold and Kreidenweis, 2002; Kazil et al., 2011; Maalick et al., 2016). However, extensive simulations with more detailed and interactive aerosol-cloud schemes are as off yet relatively sparse, mostly due to their high computational burden. Nevertheless, the need for such models is well recognized due to the significant challenges in climate modelling imposed by aerosols and clouds (Boucher et al., 2013). In particular, formation of drizzle and wet scavenging of aerosols and the associated feedback processes are potentially very important for the dynamics and circulation structures of marine stratocumulus clouds (Wang et al., 2010; Wood and Bretherton, 2004; Wood et al., 2012; Terai et al., 2014). Correctly capturing the interactions between aerosol-cloud microphysics and cloud dynamics requires highly detailed microphysical schemes. Moreover, scavenging processes, depending on particle composition and size, are overall rather poorly understood and therefore poorly represented in general circulation models (Boucher et al., 2013; Croft et al., 2010). Yet, wet scavenging of aerosols may crucially affect e.g. the transport of black carbon aerosols from polluted environments to the polar areas (Garrett et al., 2011), where it has the potential to significantly affect the future change in arctic temperatures.

Besides cloud processes, another set of topics under research by the LES community is related to the formation and evolution of fogs and the effects of aerosols therein. During the last decades, a clear decrease has been observed in fog occurrence throughout Central Europe (Vautard et al., 2009; Giulianelli et al., 2014). This has occurred together with improved air quality due to decreasing trend in sulfur emissions, especially in the case of dense fogs, but this far, a quantitative connection has not been established (van Oldenborgh et al., 2010). Although in many ways driven by the same principles as clouds, fogs also feature many different aspects (Nakanishi, 2000; Gultepe et al., 2007). For example, while cloud droplets are mainly formed at the height of the peak saturation ratio at cloud base, in radiation fogs, one of the most common fog types, the droplet formation is primarily driven by radiative cooling at the top of the developing fog layer or by high supersaturation inside the fog induced by turbulence. Thus there are also marked differences related to the dynamics of the fog layer and it's life cycle as compared to clouds (Porson et al., 2011). Fog properties and their occurrence are strongly affected by aerosol properties and anthropogenic emissions (Bott, 1991; Kokkola et al., 2003; Stolaki et al., 2015; Maalick et al., 2016), although many of the details of these interactions remain poorly understood. Improved knowledge can be pursued through increasingly sophisticated microphysical schemes embedded in LES models.

Here, an innovative approach is proposed to treat the issues related to microphysical interactions between aerosols and clouds within a high-resolution LES model. We build and extend upon state-of-the-art LES and sectional microphysical models (Stevens et al., 2005; Kokkola et al., 2008) to create a cloud-resolving framework, where the size distributions of aerosols,

Geosci. Model Dev. Discuss., doi:10.5194/gmd-2016-159, 2016
Manuscript under review for journal Geosci. Model Dev.
Published: 6 July 2016

clouds and drizzle are all described with a detailed, fully interactive sectional approach. In particular, the model introduced in this work accurately preserves the characteristics of the aerosol size distribution both in- and outside of clouds and fogs, making it ideal for studying the impact of removal processes, cloud processing and evaporation on the particle size distribution, as well as the associated feedbacks on cloud properties, drizzle formation and fog life cycle. The model is evaluated by experimenting on two very different cases: one comprising marine stratocumulus clouds based on the well-characterized DYCOMS-II dataset (Stevens et al., 2003), and another focusing on a radiation fog event based on the findings of (Porson et al., 2011; Price, 2011). The results are compared with earlier studies and previous model versions and similarities and differences are analyzed and explained in detail.

The new model is described in detail in Section 2 while case descriptions and results for the marine stratocumulus and fog cases are documented in Sections 3 and 4, respectively. Discussion of the model performance and conclusions drawn from the results are reported in Section 5.

2 Model description

2.1 The extended SALSA module

The Sectional Aerosol module for Large Scale Applications (SALSA; Kokkola et al. (2008)) is used as the basis for developing a unified sectional microphysical model for aerosols, clouds and drizzle/rain. The SALSA module, previously employed in the ECHAM (Stevens et al., 2013) climate model family, discretizes the aerosol size distribution into 10 size bins according to the dry particle diameter as shown in Figure 1 (Bergman et al., 2012). The total diameter range covered by the bins (from 3 nm to 10 μm by default) is divided into subranges 1a and 2a. This division into subranges aims at minimizing the number of tracer variables. This is achieved by including only those chemical compounds that are significantly abundant in each subrange. Subrange 1a covers the three smallest bins (up to 50 nm) and the particles are assumed to be internally mixed being composed of compounds that contribute to the growth of newly formed particles, i.e. sulfate and organic carbon. Subrange 2a includes particles larger than 50 nm whose composition may comprise all the chemical compounds in the model. The module can be configured to include 7 additional bins (designated 2b) parallel to the bin regime 2a, which allow the description of externally mixed particle populations so that soluble compounds are emitted to 2a while insoluble compounds are emitted to 2b. Further details about the bin layout can also be found in Laakso et al. (2016). The spectral resolution given by this bin layout is quite coarse, but does provide a good compromise between computational cost and model performance. Note however, the numbers given here represent the default settings - the number of bins can be set larger, if necessary. The SALSA module includes detailed methods for solving the key microphysical processes; coagulation, condensation of aerosol precursor gases (sulphate, organics) as well as new particle formation by sulphuric acid. A detailed description of the methods for solving aerosol microphysical processes is given by Kokkola et al. (2008, 2014).

Geosci. Model Dev. Discuss., doi:10.5194/gmd-2016-159, 2016
Manuscript under review for journal Geosci. Model Dev.
Published: 6 July 2016

2.1.1 Cloud droplets

In the new extended SALSA, additional size sections for cloud droplets and drizzle are implemented (Figure 1). Strictly speaking, to reproduce the evolution of the aerosol size distribution through cloud processing and wet scavenging by precipitation accurately, which is the goal of this work, a two dimensional dry/wet diameter bin system would be required. This is because cloud activation depends essentially on the dry aerosol size distribution, while collision processes and deposition rates depend strongly on the wet particle size. However, the two-dimensional framework is not a computationally feasible approach for applications such as large-eddy modelling. As a compromise between accuracy and computational burden, a unique strategy is proposed, where the cloud droplet bins are defined to be parallel to the aerosol bins (specifically, the 2a/b-bins by default) in terms of the dry diameter of the activated cloud condensation nucleus (CCN). This way, the properties of the aerosol size distribution are preserved upon cloud droplet activation, as well as evaporation of cloud droplets, though subject to the typical uncertainties inherent to the sectional approach (Khain et al., 2015).

In the extended SALSA, condensation of aerosol precursors as well as water vapour is solved for all particles and droplets using the analytical predictor method for condensation (Jacobson, 2005). However, for water vapour below a relative humidity (RH) of 98 %, the wet size of aerosol particles is determined as an equilibrium solution based on the molalities of different particle species (Kokkola et al., 2008; Stokes and Robinson, 1996), and the analytical predictor for condensation is solved above 98 % RH. The division of the water vapor condensation process is necessary due to the very fast relative changes in aerosol water content especially in subsaturated conditions and with small particles. Even close to saturation, a very small timestep ($\ll$ 1 s) is required for non-oscillatory solutions with small aerosol particles, which is not practical for the applications of this work. As a solution, a simple substepping method is employed in the condensation procedure, which takes approximately 50 substeps for every host model timestep (typically around 1 s).

Two methods are available for simulating the formation of cloud droplets in the extended SALSA. One is the parameterization by Abdul-Razzak and Ghan (2002), which takes as an input the aerosol properties and updraft velocity (along with atmospheric thermodynamic properties) to determine the maximum supersaturation in a parcel of air and thus the critical particle diameter for activation. Another is based on resolving the wet aerosol particle diameter: once the wet diameter of a particle exceeds the critical diameter corresponding to the resolved supersaturation from the host model, the particle is activated. Since the condensation of water vapour is solved dynamically for high RH, it is preferable to use the latter approach instead of the parameterized one for consistency in terms of the peak supersaturation. This also allows cloud activation in other parts of the cloud than the cloud base, e.g. due to radiative cooling effects at the cloud top or supersaturation caused by mixing of airmasses. However, if the vertical resolution of the host model is coarse (several tens of meters and above) it becomes necessary to use the parameterized method. With coarse resolution the supersaturation peak at cloud base may be underestimated due to averaging effects, which yields underestimated cloud droplet number concentration (CDNC).

The relatively coarse spectral resolution of the aerosol bins may induce unwanted discontinuities in the cloud activation calculation due to the particle size discretization. To mitigate these effects, the extended SALSA accounts for the distribution

Geosci. Model Dev. Discuss., doi:10.5194/gmd-2016-159, 2016
Manuscript under review for journal Geosci. Model Dev.
Published: 6 July 2016

of particle number and mass within the critical aerosol size bin using linearly fitted slopes between the bin centres (Korhonen et al., 2005) with both of the available methods for cloud activation.

Evaporation and deactivation of cloud droplets is accounted for through the resolved condensation, upon which activated aerosol particles are released back to the aerosol bin regime as illustrated in Figure 1. For this to take place, a very simple diagnostic is used, where subsaturation with respect to water vapour is required and the cloud droplet diameter should be smaller than 20 % of the critical diameter dictated by the properties of the CCN (or 2 μm at maximum). These thresholds were obtained by physical reasoning and experimentation with the model.

2.1.2 Drizzle

Due to our strategy of defining the cloud droplet size bins according to the dry CCN size, the wet radius of the droplets represents a mean inside each size bin. Although the droplet size can be expected to be somewhat correlated with the dry CCN size, not knowing the wet droplet diameter exactly yields an obvious setback when predicting the mass and number of particles considered as drizzle. Therefore, a type of autoconversion parameterization is formulated. Here, a lognormal distribution (selected because of mathematical simplicity) is assumed to describe the variation of the droplet wet size within each cloud droplet bin. The mode diameter is given by the bin mean cloud droplet wet diameter and the geometric standard deviation is set as $\sigma_g^{ac} = 1.2$, which results in a relatively narrow distribution and is similar to the values used for cloud droplet size distribution in the default UCLALES. Setting a commonly used threshold diameter for drizzle droplets, $d_0 = 50$ μm, the number and mass concentrations of newly formed drizzle from the cloud droplet bins are obtained as an integral over the lognormal distribution from d_0 upwards.

The evolution of the drizzle droplet population is described with an additional set of size bins (Fig. 1). However, since the growth of the drizzle droplets through condensation and collection processes is critical to produce realistic surface precipitation rates, the drizzle size bins are defined according to the wet droplet diameter, different from the cloud and aerosol size bins. This is in contrast with our emphasis of tracking the aerosol size distribution properties, but is an acceptable compromise, since the number concentration of drizzle droplets is always much smaller than the concentration of cloud droplets or aerosols. Thus, their influence on the shape and chemical composition of the ambient aerosol size distribution upon droplet evaporation is not considerably obscured by the averaging effects acting on the properties of the aerosol particles embedded inside the drizzle droplets. The drizzle bins cover the size range from 50 μm to 2 mm. This range is divided into 7 sections with strongly non-uniform spectral resolution: the width of the smallest bins is 5 μm and 1 mm in the largest bins.

The efficiency of rain collection of particles of different sizes is determined by coagulation kernels, for which Brownian diffusion with convective enhancement and gravitational settling are implemented. Aerosol particles collected by drizzle or rain drops accumulate the aerosol mass inside the drizzle bins. Upon evaporation of a drizzle droplet, it is assumed that a single particle is released and it is placed in an aerosol bin with mean diameter closest to the released dry particle size.

Geosci. Model Dev. Discuss., doi:10.5194/gmd-2016-159, 2016
Manuscript under review for journal Geosci. Model Dev.
Published: 6 July 2016

2.2 Coupled UCLALES-SALSA

The UCLALES (Stevens et al., 2005) model is a large-eddy model based on the Smagorinsky-Lilly subgrid model. In the doubly periodic domain, advection of momentum variables is based on a fourth order difference equation with time-stepping by the leap-frog method. For scalars, simple forward timestepping is used. Prognostic variables in the UCLALES are the three wind components u, v, and w (with the standard meteorological notation), liquid water potential temperature θ_l and total water mixing ratio r_t, plus some additional prognostic scalars depending on the selected thermodynamic level (e.g. rain water). UCLALES contains three thermodynamic levels, which comprise dry, moist and precipitating thermodynamical models, the latter two of which are based on the saturation adjustment method.

Coupling the extended SALSA module into UCLALES yields extensive changes in the thermodynamic core of the model as compared to the default version, thus adding a new thermodynamic level (Level 4). With the coupled UCLALES-SALSA, condensation of water vapour on cloud droplets and aerosols is explicitly computed. Therefore, instead of r_t in case of the saturation adjustment method, Level 4 treats water vapour r_v and condensate r_c mixing ratios as separate prognostic variables. This allows non-equilibrium conditions with respect to water vapour, in contrast to the default UCLALES. θ_l is retained as a predicted variable, which allows simple treatment of the latent heat transfer during moist adiabatic transitions.

UCLALES has an option to calculate cloud interaction with radiation using a four-stream radiative transfer solver (Fu and Liou, 1993). The radiation calculation takes as an input the total number concentration of cloud droplets and the cloud water content. With UCLALES-SALSA, the total number of droplets and condensate mass are obtained as the sum over the cloud droplet size bins and used to calculate radiative transfer the same way as in the default UCLALES.

The particle number concentrations as well as the masses of different compounds (aerosol species, liquid water) in each particle size bin constitute a prognostic variable, raising the number of prognostic scalars to $\mathcal{O}100$ even with a simple sulphate-based setup. This obviously has an impact on the computational burden - the model runs at about real-time with a Cray XC30 supercomputer. While this is a substantial constraint on the applicability of the model, short 12-24 hour (model time) simulations are feasible and in the following sections we will show that the presented methods are necessary to improve our understanding about boundary layer clouds, fogs and aerosols.

3 DYCOMS-II

3.1 Case description and model configuration

The new UCLALES-SALSA is first configured and tested based on the case DYCOMS-II flight RF02 (Stevens et al., 2003), which took place off the coast of California in July, 2001. The observations conducted in this case featured a mix of open and closed cell stratocumulus structures, with strong drizzle associated with the first. For the model setup we follow the settings defined by Ackerman et al. (2009): In all simulations, the initial profiles of liquid water potential temperature θ_l, total water mixing ratio r_t (taken as supersaturated vapour in the model initialization process), and u and v wind components were

Geosci. Model Dev. Discuss., doi:10.5194/gmd-2016-159, 2016
Manuscript under review for journal Geosci. Model Dev.
Published: 6 July 2016

specified with the following equations.

$$\theta_l = \begin{cases} 288.3\ \mathrm{K} & z < z_i \\ 295 - (z - z_i)^{1/3}\ \mathrm{K} & z \geq z_i \end{cases} \quad (1)$$

$$r_t = \begin{cases} 9.45\ \mathrm{g\ kg^{-1}} & z < z_i \\ 3 - 5\,(1 - \exp((z - z_i)/500))\ \mathrm{g\ kg^{-1}} & z \geq z_i \end{cases} \quad (2)$$

$$u = 3 + 4.3z/1000\ \mathrm{m\ s^{-1}} \quad (3)$$

$$v = -9 + 5.6z/1000\ \mathrm{m\ s^{-1}} \quad (4)$$

In the above, z_i is the initial inversion level set at 795 m. In addition, a large-scale subsidence rate of $3.75 \times 10^{-6}\ \mathrm{s^{-1}}$ is assumed, together with prescribed latent and sensible heat fluxes of 93 and 16 $\mathrm{W\ m^{-2}}$.

The simulations span 10 hours, the first hour of which is considered as the spinup period. In UCLALES-SALSA, drizzle formation and coagulation of particles are not allowed during this period in order to prevent spurious effects on the cloud properties during the initial buildup of turbulent kinetic energy (TKE) and settling of the boundary layer properties. The simulation domain spanned 5 km into each horizontal direction and 1600 meters in the vertical, with the topmost 200 meters used as a sponge layer, damping unrealistically reflected gravity waves at the model top. The horizontal resolution is set to 50 m while the vertical resolution is 20 m. A more detailed description of the model experiments is given below and their key aspects are summarized in Table 1. The performance of the UCLALES-SALSA model is evaluated by comparing the results with those from the default UCLALES. This can also be contrasted to the model ensemble used in the LES intercomparison in which the default UCLALES was a part of (Ackerman et al., 2009). Thus we can isolate and characterize the effects induced by the use of an elaborate sectional microphysical scheme for aerosols and clouds.

3.1.1 Default case experiments

The default experiments are based on the basic settings in terms of aerosol and cloud microphysics. For the experiment performed with UCLALES-SALSA, designated as LEV4, this means that we use the two-mode lognormal initial aerosol size distribution given in Ackerman et al. (2009), which is assumed to consist of sulphate aerosol. The total number, geometrical mean diameter and geometrical standard deviation are 125 $\mathrm{cm^{-3}}$, 22 nm and 1.2 for the first mode and 65 $\mathrm{cm^{-3}}$, 120 nm and 1.7 for the second mode. In the model initialization, the size distribution is remapped into the SALSA aerosol size bins. For comparison with the experiment LEV4, a parallel experiment, designated LEV3, is performed with the default UCLALES configuration, including moist thermodynamics and drizzle. However, since the default UCLALES does not contain a description for aerosols, the CCN number concentrations must be prescribed, similar to most other available LES models. In LEV3, the CCN concentration is set as 55 $\mathrm{cm^{-3}}$, which roughly corresponds to the number of cloud droplets initially produced by LEV4 and is also the number used in other LES simulations based on this particular case (Ackerman et al., 2009; Savre et al., 2014).

Geosci. Model Dev. Discuss., doi:10.5194/gmd-2016-159, 2016
Manuscript under review for journal Geosci. Model Dev.
Published: 6 July 2016

3.1.2 Sensitivity tests

A set of sensitivity tests are performed to further investigate certain aspects of the model. Experiments designated as LEV4HI and LEV3HI are performed. These are similar to LEV4 and LEV3, but with higher aerosol (or CCN for LEV3HI) concentration (mode number concentrations multiplied by 3), and are utilized to study how the coupling between the model microphysics and dynamics reacts to perturbations in the initial aerosol and cloud properties.

3.2 Results

3.2.1 General features

Figure 2 shows a domain mean time-height plot of the liquid water content (LWC) in the LEV3 and LEV4 experiments. While in the early stages of the simulation the LWC and the macroscopic cloud structure are quite similar between LEV3 and LEV4, after about 4 hours the results start to diverge substantially, marking a clear shift in the boundary layer dynamics. Whereas LEV3 simulations maintain a solid stratocumulus deck until the end of the simulated period, LEV4 results in a very thin stratiform cloud deck just below the inversion with low LWC and only 5-10 cm^{-3} cloud droplets. However, this setting is interspersed by occasional deeper and more massive shallow convective cumulus elements. This is reminiscent of the formation of open cell circulation structures in marine Sc clouds (Wood and Hartmann, 2006), which were also observed during RF02 (Stevens et al., 2003).

Figure 3 shows the total liquid water path (LWP, taken as cloud droplets plus drizzle) and the rain water path (liquid water interpreted as drizzle in the model) for LEV3 and LEV4. Again, the LWP is fairly similar between the two experiments during the first 4 hours, after which LEV4 starts to deviate from LEV3. However, in a later stage, substantial portion of the total LWP is interpreted as drizzle in LEV4, while in LEV3 the water mass considered as drizzle is much smaller. This is seen mainly as a diagnostic discrepancy: in LEV4 most of the excess drizzle droplets reside within the cloud layer in the smallest drizzle bin, which do not yet exhibit notable fall speeds and are evaporated quickly after descending below the cloud layer. This stems from the details in parameterizing drizzle formation. Differences arise for example from the fact that when large cloud droplets are considered as drizzle in UCLALES-SALSA, they are transferred to the smallest drizzle bin, beyond which their growth is explicitly modelled (though subject to low bin resolution). Instead in LEV3, a size distribution (based on gamma function) is assumed for the drizzle droplets, which causes at least a part of the drizzle amount to reach surface-reaching size range very quickly compared to LEV4. Figure 4a shows that despite the difference in the drizzle water path, the surface precipitation rate is of similar order of magnitude between LEV3 and LEV4 (after considering the spinup period). This is used as the main criterion for setting up the model parameters such as σ_g^{ac} for the basic experiments. Nevertheless, even after considering the differences in drizzle amount, it is evident, that the boundary layer and cloud properties in LEV4 shift towards a very different state as compared to LEV3.

Geosci. Model Dev. Discuss., doi:10.5194/gmd-2016-159, 2016
Manuscript under review for journal Geosci. Model Dev.
Published: 6 July 2016

3.2.2 Boundary layer structure

In the LEV4 experiment, the boundary layer shows somewhat more stratified characteristics than that in LEV3. Figure 5 plots the domain mean vertical profiles of potential temperature, water vapour and liquid water mixing ratios. Especially towards the end of the simulation, LEV4 shows a rather distinct division of the boundary-layer into two separate mixing regimes. This decoupling of the cloud-driven layer (see for reference the conceptual models e.g. in Harvey et al. (2013)) is evident in both the potential temperature as well as water vapor mixing ratio, with the sharpest gradient taking place around $400\ \mathrm{m}$ height, following the criteria defined in Jones et al. (2011). In LEV3 the temperature profile is weakly stable as well after 9 hours of simulation, but less so than in LEV4. In particular, the water vapor mixing ratio in LEV3 does not show the same separation as LEV4.

It is typical for a stratocumulus topped boundary layer to shift towards a decoupled structure in the morning as shortwave heating by the rising sun begins to offset the longwave cloud top radiative cooling and therefore reduces cloud driven mixing (Ghate et al., 2014). Although wind shear may also affect the entrainment and cloud top static stability (Wang et al., 2012), it is not surprising that the sharpest transition in LEV4 occurs around 5 hours into the simulation, which is also close to sunrise at the assumed location. It is also noted that after the initial shift, the decoupled structure is subject to positive feedbacks as it reduces the supply of moisture from the surface to the cloud layer, which further reduces the cloud top radiative cooling and thus the cloud driven mixing. This also weakens the cloud top inversion, allowing transport of heat to the upper mixed layer by entrainment. Due to the stable layer at the decoupling interface, heat transferred to the cloud-driven layer is not efficiently mixed, resulting in even more pronounced decoupling of the cloud layer. By the same token, a larger portion of moisture released from the surface by the latent heat flux is confined to the surface layer, thus contributing to the relatively high water vapour mixing ratio in LEV4 as compared to LEV3.

3.2.3 Role of microphysics and drizzle

Even though LEV3 and LEV4 simulations are subject to identical external forcings, LEV3 does not show as abrupt changes in the simulated cloud layer nor the boundary-layer structure as LEV4 does, indicating that something makes the LEV4 boundary-layer more susceptible to undergo the decoupling process. As discussed next, the reason for the initial perturbation towards this different state can be traced back to the representation of microphysics and drizzle. Figure 4 shows the surface precipitation rate in LEV3 and LEV4 simulations as well as the rate of removal of sulphate aerosol embedded inside precipitating droplets, illustrating the models ability to resolve the aerosol wet scavenging process. The UCLALES-SALSA performs this task with very high detail: the size distribution of aerosols is preserved through activation scavenging, beyond which droplet growth and subsequent drizzle generation favors large soluble particles.

The reduction in aerosol number concentration due to cloud activation in LEV4 is clearly visible immediately after the model initialization in Figure 6. After a couple of hours of drizzle formation in LEV4, the consequences of aerosol scavenging by activation and drizzle fallout become visible in the below cloud layer as the aerosol number concentration decreases quite rapidly both in the cloud and in the below-cloud layers. Since the scavenging is size resolved, and favors larger particles,

Geosci. Model Dev. Discuss., doi:10.5194/gmd-2016-159, 2016
Manuscript under review for journal Geosci. Model Dev.
Published: 6 July 2016

the number of potential CCN and thus CDNC is strongly reduced with time. This supports continuing production of drizzle droplets, which eventually cover a considerable fraction of the total droplet concentration within the stratiform cloud layer. The scavenging of particles and the consequent reduction in cloud water content start to weaken cloud top radiative cooling already during the first few hours of the simulation in LEV4. In contrast, in LEV3 such transition towards thinner cloud layer with lower cloud water content does not take place, because of the lack of representation for aerosol scavenging.

Because of the low aerosol concentration and sufficient amount of water available in the model initial state, the presented case favors considerable drizzle production. Considering the interactive description of particles and the detailed aerosol removal mechanisms included in the model, the results shown here are not scientifically surprising, but are used to demonstrate the model's ability to reproduce the transitions in boundary-layer and cloud structure due to microphysical interactions. Interestingly, the LEV4 results on LWP and rain water path show quite similar features as those obtained with a cloud system resolving model with interactive aerosols (Yamaguchi and Feingold, 2015). However, UCLALES-SALSA provides the means for more detailed investigations about the impact of particle size distribution and composition on cloud dynamics and aerosol-cloud interactions, which justifies the added complexity and computational demand. This is demonstrated in more detail by Figure 7, showing the relative change in particle number concentrations for individual bins (combining both non-activated aerosol and activated CCN particles) in the in-cloud and below-cloud layers. It is shown that after the spinup period in the below-cloud layer, the smaller particles are removed by precipitation collection and, in part, also by activation in air parcels caught in updrafts. However, the number of the largest particles present increases, which is due to evaporating drizzle below the cloud. These droplets have had time to collect additional aerosol mass during their growth, which upon the droplet evaporation is released as a single large particle, preserving the mass of the aerosol. Note that while the relative change appears large, the initial number of particles in these bins is relatively small, about $1 - 10\ \mathrm{cm}^{-3}$. Inside the cloud the particles are removed by activation, cloud collection and the subsequent wet deposition. Since the UCLALES-SALSA includes a variety of processes that directly influence the size distribution and composition of aerosol particles, this also affects the distribution and variation of the mass of soluble material inside cloud droplets. This, at least in the initial phase of droplet formation, contributes to the their growth rate which may affect drizzle formation. In this context, the detailed description of the evolution of the aerosol size distribution provided by the model also enables the investigation of aerosol particle emissions, e.g. giant sea salt particles, and their influence on the cloud properties and drizzle.

3.2.4 Impact of initial particle concentration

Since it is apparent that drizzle formation and the subsequent impacts of particle scavenging yield the divergence of results between the LEV3 and LEV4 simulations, it is necessary to test how changing the particle number concentrations affects the results. This is done simply by repeating the LEV3 and LEV4 experiments with particle concentrations multiplied by three, designated as LEV3HI and LEV4HI. With higher particle concentrations, the precipitation reaching the surface is very small or non-existent in both simulations, which suppresses the wet scavenging effect in LEV4HI. As a result, the cloud properties in LEV4HI remain quite close to those in LEV3HI during the simulated period. This is seen in the domain mean profiles of LWC and the boundary layer thermodynamical properties, shown in Figure 8, which are indeed remarkably similar between the two

Geosci. Model Dev. Discuss., doi:10.5194/gmd-2016-159, 2016
Manuscript under review for journal Geosci. Model Dev.
Published: 6 July 2016

experiments. This shows that in conditions where the additional processes and interactions in the new UCLALES-SALSA are not dominating the boundary-layer and cloud evolution, the results remain physically consistent with the more simple model versions. It should be noted though, that if the LEV4HI simulation would be continued over an extended period of time, the supply of moisture by the (constant) latent heat flux and the effects of cloud processing and coagulation on the aerosol size distribution would eventually create drizzle and rain, which would then lead to a similar situation as seen in the experiment LEV4. It has been shown that maintaining a steady-state cloud structure requires aerosol replenishment from multiple sources, including aerosol emissions (Wood et al., 2012). Although there is some aerosol replenishment through mixing from the free atmosphere in our model experiments, this is not enough to maintain the cloud deck over prolonged periods of time. Considering the outcomes of the experiments LEV4 and LEV4HI, the model results here are consistent with the findings of Jiang and Wang (2014) regarding the effects of aerosol replenishment. Thus, implementation of aerosol emissions into UCLALES-SALSA is part of our future plans.

4 Simulating fog formation and evolution

4.1 Case description and model configuration

To demonstrate the versatility of UCLALES-SALSA, the model is configured according to the conditions from a radiation fog event that took place at the UK Met Office research site at Cardington in the night of $12-13^{\mathrm{th}}$ of February, 2008 (Porson et al., 2011; Price, 2011). Simulations using different aerosol concentrations and horizontal wind profiles are introduced to illustrate the potential effect of aerosol and wind shear on the properties of radiation fog.

Here, the model is run with a very high resolution, vertically spanning $1.5\ \mathrm{m}$ in the lowest $150\ \mathrm{m}$. Above, the resolution is gradually decreased so that model top is at approximately $800\ \mathrm{m}$ with total number of levels being 165. The horizontal resolution is $4\ \mathrm{m}$ in each direction and the domain covers an area spanning $320\ \mathrm{m}$ by $640\ \mathrm{m}$. The settings for microphysics in the UCLALES-SALSA run are kept similar to those used in the DYCOMS-II case (Section 3), with the exception that drizzle formation was switched off in the fog simulations and the sedimentation of cloud droplets was the main sink of cloud water. While droplet number concentrations were prescribed in the simulations performed by Porson et al. (2011), here, droplet activation is computed based on the growth of the aerosol particles to larger than their critical radius at water vapour supersaturation resolved by the model. This is important since in radiation fogs the droplet formation is mainly driven by the radiative cooling at the top of the fog layer. Solving the condensation equation also allows the evaporation of cloud droplets inside the fog if supersaturation falls below the water surface pressure in the smallest cloud droplet bins. This process can reduce the number of droplets and has been found to take place also in clouds (Wood et al., 2002; Romakkaniemi et al., 2009).

In contrast to the experiments in Section 3, the surface heat fluxes are not prescribed, but are determined with a simple parameterization for soil energy balance, which is coupled with the radiation scheme (Ács et al., 1991). Moreover, the heat transfer between surface and deeper soil is approximately taken into account (Ács et al., 1991). For the latent heat flux the surface is assumed to be saturated with respect to water. This can be assumed to be a fairly good approximation until the fog dissipation phase, when the evaporation from warming surface can deplete the water from surface layer and the assumption of

Geosci. Model Dev. Discuss., doi:10.5194/gmd-2016-159, 2016
Manuscript under review for journal Geosci. Model Dev.
Published: 6 July 2016

saturated surface may overestimate the latent heat flux. Due to the simplicity of the surface energy balance model, the surface heat capacity is used as a tunable parameter to reproduce reasonable surface cooling rate in comparison with observations.

The impact of aerosols on fog formation is first investigated by three parallel experiments with zero initial horizontal wind velocities, which differ in their initial particle concentration. As the information of aerosol concentration is not available for the chosen simulation, we use bimodal aerosol size distribution with mean sizes of $50\ \mathrm{nm}$ and $150\ \mathrm{nm}$. In all simulations the number concentration in Aitken mode is kept in 1000 cm^{-3} while the number of accumulation mode aerosols is increased consecutively so that the accumulation mode particle concentrations are 200, 400 and $800\ \mathrm{cm}^{-3}$ in experiments A200, A400 and A800, respectively. An additional experiment, A400W is then presented, where the model is initialized with the horizontal wind data from (Porson et al., 2011).

4.2 Results

Similar to the observation-based reports by Price (2011) and LES studies (Nakanishi, 2000; Porson et al., 2011), the fog layer investigated here undergoes distinct thermodynamical transitions during its evolution. Initially, the fog forms near the surface in a very stable layer due to the longwave cooling effect. As the fog-layer encroaches upwards and more droplets are activated at the fog top layers, its optical thickness increases which reduces the radiative cooling effect at the surface. At the same time the peak of radiative cooling at the fog top region becomes more pronounced. Figure 9 shows the evolution of the fog droplet concentration (sampled at 10 meters height) and the growth of the fog layer thickness. For the experiments A200, A400 and A800 (initialized with zero horizontal wind) the increase in the number of droplets due to increasing aerosol concentration is clearly seen. Higher initial aerosol concentration yields increased fog layer depth, but the differences between the experiments are minor. This is due to the stability of the temperature profile, which suppresses the mixing especially with low aerosol concentration, as show in Figure 10.

In the early morning there is a transition from stable to almost neutral temperature stratification inside the fog. Higher aerosol concentrations promote increased optical thickness of the fog layer, which leads to faster formation of the neutral temperature profile. This is qualitatively similar to the results presented in Price (2011) and is attributed to the reduction in the surface longwave cooling effect with optically thick fog layers and to the supply of heat from the soil. As can be seen from Figure 9, the earlier formation of a neutral temperature profile with higher aerosol load further enhances the aerosol effect on fog droplet concentration (04 UTC in A800) through a positive feedback similar to what has been found to take place at the top of fog, where the increase in droplet concentration enhances radiative cooling which again feeds back as a higher supersaturation and enhanced particle activation (Maalick et al., 2016). Figure 11 shows the profiles of radiative cooling rate and the water vapour supersaturation as a function of time for the three experiments. As expected, the peak radiative cooling is indeed found near the top of the fog layer. Moreover, the intensity of the cooling increases with increasing aerosol concentration, owing to the higher optical depth: in A800 the peak cooling rate is approximately $7\ \mathrm{K\,hr}^{-1}$ and in A200 $4\ \mathrm{K\,hr}^{-1}$. This is in agreement with the range of values reported in Nakanishi (2000). The peak water vapour supersaturation is found at the same altitudes as the strongest radiative cooling. However, larger particle concentration depletes the available water vapour more efficiently, resulting in highest supersaturation to occur with the lowest particle concentrations.

Geosci. Model Dev. Discuss., doi:10.5194/gmd-2016-159, 2016
Manuscript under review for journal Geosci. Model Dev.
Published: 6 July 2016

These findings illustrate the ability of the UCLALES-SALSA to provide a realistic description of not only the thermodynamic and microphysical properties of fogs, but also the aerosol-fog-radiative interactions and feedbacks. The results from the experiments A200, A400 and A800 compare quite well with those reported in Porson et al. (2011). This includes the rate of growth of the fog layer depth, despite the fact that their simulations were initialized with the horizontal wind profiles. However, the growth rate is considerably lower than the observed, where the fog top reaches about a $100\ \mathrm{m}$ within 7 or 8 hours from the first appearance of the fog (see figure 5 in Porson et al., 2011). For UCLALES-SALSA, this is presumably because of the lack of shear generated turbulence. Wind shear has been shown to be very important in controlling the turbulence characteristics inside radiation fogs (Bergot, 2013). Thus, in the additional experiment A400W, the UCLALES-SALSA is initialized with an approximately similar wind profile as in (Porson et al., 2011). Interestingly, in this case the growth of the fog layer corresponds much more closely to the observed, as shown by the dashed line in Figure 10. The wind shear present in A400W (Figure 12) yields vertical mixing, which strongly enhances the droplet production within the fog layer even at the initial phase (Figure 9). The mixing and perturbations in radiative heating, as compared to the zero-wind experiments, produce the neutral temperature stratification quite quickly and the strength of the inversion at the top of the fog is also slightly reduced, as shown by Figure 12. This allows more rapid growth of the fog layer, the depth of which reaches over $150\ \mathrm{m}$ by morning. This is even deeper than suggested by the observations, and can be attributed to e.g. missing advection effects or possible differences in the initial moisture or temperature profiles. At the same time the increased mixing enhances droplet activation and decreases the differences between different aerosol concentrations.

These results point towards the importance of detailed representation of the microphysical processes. In particular, the size resolving microphysics in UCLALES-SALSA does well in reproducing the fog droplet size distribution. The peak number concentrations are generally found for droplet diameters between $20\ \mu\mathrm{m}$ and $25\ \mu\mathrm{m}$, which agrees well with measurements (Price, 2011). This has many positive implications, since realistically capturing the droplet growth is important for representing the droplet sedimentation, which is an essential driver for the fog evolution. As the droplet number concentration simulated by UCLALES-SALSA also agrees quite well with observations, together these processes contribute to accurate estimation of the liquid water content and fog optical depth as well as their vertical distribution. These are then directly linked to the fog and boundary-layer dynamics. Increased fog optical depth due to increased droplet concentration will delay fog evaporation in the morning after sunrise, which thus connect the aerosol concentration into fog existence. However, to fully evaluate the aerosol effect on fog lifetime, a more detailed land surface scheme is needed to correctly simulate the latent heat flux and atmospheric water content after sunrise.

5 Conclusions

A new large-eddy simulation model coupled with a fully interactive bin-microphysical scheme for aerosols and clouds was presented. The model is based on well-established components: the UCLALES large-eddy simulation model and the SALSA aerosol model, extended with cloud droplets and drizzle. The bin system for aerosols and clouds follows a unique approach, where the size bins are defined according to the dry particle size for both activated and non-activated particles in an attempt

Geosci. Model Dev. Discuss., doi:10.5194/gmd-2016-159, 2016
Manuscript under review for journal Geosci. Model Dev.
Published: 6 July 2016

to hold detailed information about the aerosol size distribution both in ambient air and within clouds. This also enables an elaborate description of the effects of cloud processing on the properties of the aerosol population as well as a size and composition-resolved simulation of the wet scavenging of aerosols.

The model was tested and evaluated using two well-characterized cases: one comprising marine stratocumulus clouds from the DYCOMS-II campaign and another based on measurements of a radiation fog event in Cardington, UK. For the stratocumulus experiments, the UCLALES-SALSA initially produced very similar cloud and boundary layer properties as other LES model versions, many of which rely on bulk microphysics and prescribed particle or droplet concentrations. However, after about 5 hours, UCLALES-SALSA shifted towards a very different boundary-layer state, as compared to the default LES, resulting in a thin stratiform cloud deck at the top of a decoupled layer instead of a solid stratocumulus cloud layer. This shift was attributed to the wet removal of aerosol particles with drizzle, which eventually led to a decrease in cloud droplet number and water content. This enhanced the susceptibility of the boundary layer to undergo a significant decoupling when triggered by the change in radiation budged during sunrise, which then yielded even more dramatic shift in the cloud properties, forming a feedback loop. Such behavior was not reproduced by the default UCLALES nor by most of the models used in Ackerman et al. (2009), which is due to prescribed microphysical properties and lack of interactions treated by the model. While the transition in the cloud properties simulated by the UCLALES-SALSA resembles that related to closed-to-open cell transitions in marine stratocumulus, it is noted that the rather small model domain (5×5 km) is much too small to represent the circulation dynamics and feedbacks closely related to the real-world mesoscale morphological transitions. Nevertheless, the results are encouraging and show that the model may very well provide the necessary new information related to aerosol-cloud-drizzle interactions in future studies to explain the observed stratocumulus characteristics.

In another set of experiments, the skill of the model in simulating fog formation and development was shown. The model was able to capture the evolution of the fog radiative properties and the resulting changes in the thermodynamical profiles. While increasing the initial aerosol concentration had only slight impact on the growth of the fog layer depth, larger particle concentration did clearly affect the rate of evolution of the temperature profile, which showed a transition from very stable conditions to eventually almost neutral profile. This is qualitatively in agreement with the observed behavior Price (2011). While the growth of the fog-layer depth was clearly underestimated, as compared to observations, when the model was initialized with zero wind speeds, setting a realistic wind profile resulted in a growth rate very similar to the observations. With horizontal wind present, the formation of a neutral temperature stratification is even more pronounced than with zero wind conditions, and even more resembles the observed properties. Porson et al. (2011) identified advection and drainage flows as plausible explanations for the discrepancy between their model and observations. The results presented in this study also bear these deficiencies and are also affected by other shortcomings, such as the surface scheme which is most likely over simplified. The remaining differences between the radiation fog simulated by UCLALES-SALSA and the observations notwithstanding, the results of this study still make a strong point for a very detailed representation of aerosol and cloud microphysics in simulating the fog evolution.

The need for high-resolution models that can accurately simulate the interactions between aerosols and clouds in both ways and couple these effects to the dynamical features of the atmosphere is clearly highlighted by the current challenges e.g. in

Geosci. Model Dev. Discuss., doi:10.5194/gmd-2016-159, 2016
Manuscript under review for journal Geosci. Model Dev.
Published: 6 July 2016

climate research. UCLALES-SALSA provides these abilities making it a highly sophisticated alternative to investigate the role of aerosols in marine stratocumulus clouds or fogs, or the process of wet scavenging. Although the model is currently limited to warm clouds only, implementation of ice processes is on the way and will be published in a separate paper. This will extend the repertoire of the model also towards ice and mixed-phase clouds, whose representation in climate models and the deficiencies therein have recently started to attract more widespread interest.

Code availability

The model code is available upon request and will be made more generally available by the time of release of the final version of this paper.

Acknowledgements. This work was supported by the Academy of Finland (project number 283031 and the Centre of Excellence in Atmospheric Science, 272041) and by the European FP7 project BACCHUS (Grant agreement no: 603445). We gratefully acknowledge Prof. Bjorn Stevens for providing the UCLALES code.

Geosci. Model Dev. Discuss., doi:10.5194/gmd-2016-159, 2016
Manuscript under review for journal Geosci. Model Dev.
Published: 6 July 2016

References

Abdul-Razzak, H. and Ghan, S. J.: A parameterization of aerosol activation 3. Sectional representation, J. Geophys. Res., 107, doi:10.1029/2001JD000483, 2002.

Ackerman, A. S., vanZanten, M. C., Stevens, B., Savic-Jovcic, V., Bretherton, C. S., Chlond, A., Golaz, J.-C., Jiang, H., Khairoutdinov, M., Krueger, S. K., Lewellen, D. C., Lock, A., Moeng, C.-H., Nakamura, K., Petters, M. D., Snider, J. R., Weinbrecht, S., Zulauf, M.: Large-Eddy Simulations of a Drizzling, Stratocumulus-Topped Marine Boundary Layer. Monthly Weather Review, 137, 1083-1110, DOI: 10.1175/2008MWR2582.1, 2009

Ács, R., Mihailović, D. T., Rajković, B.: A coupled soil moisture and surface temperature prediction model. J. Appl. Meteorol., 30, 812-822, 1991.

Bergman, T., Kerminen, V.-M., Korhonen, H., Lehtinen, K. J., Makkonen, R., Arola, A., Mielonen, T., Romakkaniemi, S., Kulmala, M., Kokkola, H.: Evaluation of the sectional aerosol microphysics module SALSA - implementation in ECHAM5-HAM aerosol-climate model. Geosci. Model. Dev., 5, 845-868, doi:10.5194/gmd-5-845-2012, 2012.

Bergot, T.: Small-scale structure of radiation fog: a large-eddy simulation study. Q. J. R. Meteorol. Soc., 139, 1099-1112, doi:10.1002/qj.2051, 2013.

Boucher, O. et al.: Climate Change 2013: The Physical Science Basis (eds Stocker, T. F. et al.) 571-657, IPCC, Cambridge Univ. Press, 2013.

Bott, A.: On the influence of the physico-chemical properties of aerosols on the life cycle of radiation fogs. Boundary-Layer Meteorol., 56, 1-31, 1991.

Croft, B., Lohmann, U., Martin, R. V., Stier, P., Wurzler, S., Feichter, J., Hoose, C., Heikkilä, U., van Donkelaar, A., Ferrachat, S.: Influences of in-cloud aerosol scavenging parameterizations on aerosol concentrations and wet deposition in ECHAM5-HAM. Atmos. Chem. Phys., 10, 1511-1543, doi:10.5194/acp-10-1511-2010, 2010.

Feingold, G., Kreidenweis, S. M.: Cloud processing of aerosol as modeled by a large eddy simulation with coupled microphysics and aqueous chemistry. J. Geophys. Res., 107, D23, doi:10.1029/2002JD002054, 2002.

Fu, Q., Liou, K.-N.: Parameterization of the radiative properties of cirrus clouds, J. Atmos. Sci., 50, 2008-2025, doi:10.1175/1520-0469(1993)050<2008:POTRPO>2.0.CO;2, 1993.

Garrett, T. J., Brattstrm, S., Sharma, S., Worthy, D. E. J., Novelli, P.: The role of scavenging in the seasonal transport of black carbon and sulfate to the Arctic. Geophys. Res. Lett., 38, L16805, doi:10.1029/2011GL048221, 2011.

Ghate, V. P., Albrecht, B. A., Miller, M. A., Brewer, A., Fairall, C. W.: Turbulence and radiation in stratocumulus-topped marine boundary layers: a case study from VOCALS-REx. J. Appl. Meteor. Climatol., 53, 117-135, doi:10.1175/JAMC-D-12-0225.1, 2014.

Golaz, J.-C., Wang, S., Doyle, J. D., Schmidt, J. M.: Coamps-Les: Model evaluation and analysis of second-and third-moment vertical velocity budgets. Boundary-Layer Meteorol., 116(3), 487-517, 2005.

Giulianelli, L., Gilardoni, S., Tarozzi, L., Rinaldi, M., Decasari, S., Carbone, C., Facchini, M. C., Fuzzi, S.: Fog occurrence and chemical composition in the Po valley over the last twenty years. Atmospheric Environment, 98, 394-401, 2014.

Gultepe, I., Tardif, R., Michaelides, S. C., Cermak, J., Bott, A., Bendix, J., Müller, M. D., Pagowski, M., Hansen, B., Ellrod, G., Jacobs, W., Toth, G., Cober, S. G.: Fog research: A review of past achievements and future perspectives. Pure Appl. Geophys., 164, 1121-1159, doi:10.1007/s00024-007-0211-x, 2007.

Harvey, N. J., Hogan, R. J., Dacre, H. F.: A method to diagnose boundary-layer type using Doppler lidar. Q.J.R. Meteorol. Soc., 139, 1681-1693, DOI:10.1002/qj.2068, 2013.

Jacobson, M. Z.: Fundamentals of Atmospheric Modeling, 2nd Edn., Cambridge University Press, New York, 2005.

Jiang, Q., Wang, S.: Aerosol replenishment and cloud morphology: A VOCALS example. J. Atmos. Sci., 71, 300-311, doi:10.1175/JAS-D-13-0128.1, 2014.

Jones, C. R., Bretherton, C. S., Leon, D.: Coupled vs. decoupled boundary layers in VOCALS-REx. Atmos. Chem. Phys., 11, 7143-7153, doi:10.5194/acp-11-7143-2011, 2011.

Kazil, J., Wang, H., Feingold, G., Clarke, A. D., Snider, J. R., Bandy, A. R.: Modelling chemical and aerosol processes inthe transition from closed to open cells during VOCALS-REx. Atmos. Chem. Phys., 11, 7491-7514, doi:10.5194/acp-11-7491-2011, 2011.

Khain, A. P., Beheng, K. D., Heymsfield, A., korolev, A., Krichak, S. O., Levin, Z., Pinsky, M., Phillips, V., Prabhakaran, T., Teller, A., van den Heever, S. C., Yano, J.-I.: Representation of microphysical processes in cloud-resolving models: Spectral (bin) microphysics versus bulk parameterization. Rev. Geophys., 53, 247-322, doi:10.1002/2014RG000468, 2015.

Khairoutdinov, M., Kogan, Y.: A new cloud physics parameterization in a large-eddy simulation model of marine stratocumulus. Mon. Weather Rev., 128, 229-243, 2000.

kokkola, H., Romakkaniemi, S., Laaksonen, A.: On the formation of radiation fogs under heavily polluted conditions, Atmos. Chem. Phys., 3, 581-589, doi:10.5194/acp-3-581-2003, 2003.

Kokkola, H., korhonen, H., Lehtinen, K. E. J., Makkonen, R., Asmi, A., Järvenoja, S., Anttila, T., Partanen, A.-I., Kulmala, M., Järvinen, H., Laaksonen, A., Kerminen, V.-M.: SALSA - a Sectional Aerosol module for Large Scale Applications. Atmos. Chem. Phys., 8, 2469-2483, 2008.

Kokkola, H., Yli-Pirilä, P., Vesterinen, M., Korhonen, H., Keskinen, H., Romakkaniemi, S., Hao, L., Kortelainen, A., Joutsensaari, J., Worsnop, D. R., Virtanen, A., Lehtinen, K.E.J: The role of low volatile organics on secondary organic aerosol formation. Atmos. Chem. Phys., 14, 1689–1700, doi:10.5194/acp-14-1689-2014, 2014.

Korhonen, H., Kerminen, V.-M., Lehtinen, K. E. J., Kulmala, M.: CCN activation and cloud processing in sectional aerosol models with low size resolution. Atmos. Chem. Phys., 5., 2561-2570, doi:1680-7324/acp/2005-5-2561, 2005.

Laakso, A., Kokkola, H., Partanen, A.-I., Niemeier, U., Timmreck, C., Lehtinen, K. E. J., Hakkarainen, H., and Korhonen, H.: Radiative and climate impacts of a large volcanic eruption during stratospheric sulfur geoengineering, Atmos. Chem. Phys., 16, 305-323, doi:10.5194/acp-16-305-2016, 2016.

Maalick, Z., Kühn, T., Korhonen, H., Kokkola, H., Laaksonen, A., Romakkaniemi, S.: Effect of aerosol concentration and absorbing aerosol on the radiation fog life cycle. Atmospheric Environment, 133, 26-33, 2016.

Moeng, C.-H.: A Large-Eddy-Simulation model for the study of planetary boundary-layer turbulence. J. Atmos. Sci., 41, 2052-2062, 1984.

Nakanishi, M.: Large-eddy simulation of radiation fog. Boundary-Layer Meteorol., 94, 461-493, 2000.

van Oldenborgh, G. J., Yiou, P., Vautard, R.: On the roles of circulation and aerosols in the decline of mist and dense fog in Europe over the last 30 years. Atmos. Chem. Phys., 10, 4597-4609, doi:10.5194/acp-10-4597-2010, 2010.

Porson, A., Price, J., Lock, A., Clark, P.: Radiation Fog. Part II: Large-Eddy Simulations in Very Stable Conditions. Boundary-Layer Meteorol., 139, 193-224, DOI:10.1007/s10546-010-9579-8, 2011.

Price, J.: Radiation fog. Part I: Observations of stability and drop size distributions. Boundary-Layer Meteorol., 139, 167-191, doi:10.1007/s10546-010-9580-2, 2011.

Romakkaniemi, S., McFiggans, G., Bower, K. N., Brown, P., Coe, H., Choularton, T. W.: A comparison between trajectory ensemble and adiabatic parcel modelled cloud properties and evaluation agains airborne measurements. J. Geophys. Res., 114, D06214, doi:10.1029/2008JD011286, 2009.

Saleeby, S. M., Herbener, S. R., van den Heever, S. C.: Impacts of cloud droplet-nucleating aerosols on shallow tropical convection. J. Atmos. Sci., 72, 1369-1385, doi:10.1175/JAS-D-14-0153.1, 2015.

Savre, J., Ekman, M. L., Svensson, G.: Technical note: Introduction to MIMICA, a large-eddy simulation solver for cloudy planetary boundary layers. J. Adv. Model Earth Syst., 6, 630-649, doi:10.1002/2013MS000292, 2014.

Seifert, A., Beheng, K. D.: A double-moment parameterization for simulating autoconversion, accretion and self collection. Atmos. Res., 59-60, 265-281, 2001

Seifert, A., Beheng, K. D.: A two-moment cloud microphysics parameterization for mixed-phase clouds. Part 1: Model description. Meteor. Atmos. Phys., 92, 45-66, 2006.

Stevens, B., Lenschow, D. H., Vali, G., Gerber, H., Bandy, A., Blomquist, B., Brenguier, J.-L., Bretherton, C. S., Burnet, F., Campos, T., Chai, S., Faloona, I., Friesen, D., Haimov, S., Laursen, K., Lilly, D. K., Loehrer, S. M., Malinowski, S. P., Morley, B., Petters, M. D., Rogers, D. C., Russel, L., Savic-Jovcic, V., Snider, J. R., Straub, D., Szumowski, M. J., Takagi, H., Thornton, D. C., Tschudi, M., Twohy, C., Wetzel, M., van Zanten, M. C.: Dynamics and chemistry of marine stratocumulus - DYCOMS-II. Bull. Amer. Meteor. Soc., 84:5, 579-593, doi:10.1175/BAMS-84-5-579, 2003.

Stevens, B., Moeng, C.-H. Ackerman, A. S., Bretherton, C. S., Chlond, A., de Roode, S., Edwards, J., Golaz, J.-C., Jiang, H., Khairoutdinov, M., Kirkpatrick, M. P., Lewellen, D. C., Lock, A., Müller, F., Stevens, D. E., Whelan, E., Zhu, P.: Evaluation of Large-Eddy Simulations via observations of nocturnal marine stratocumulus. Mon. Weather Rev., 133, 1443-1462, 2005.

Stevens, B., Giorgetta, M., Esch, M., Mauritsen, T., Crueger, T., Rast, S., Salzmann, M., Schmidt, H., Bader, J., Block, K., Brokopf, R., Fast, I., Kinne, S., Kornblueh, L., Lohmann, U., Pincus, R., Reichler, T., Roeckner, E.: Atmospheric component of the MPI-M Earth System Model: ECHAM6. J. Adv. Model. Earth Syst., 5, 146-172, doi:10.1002/jame.20015, 2013

Stokes, R. H., Robinson, R. A.: Interactions in aqueous nonelectrolyte solutions. I: Solute-solven equilibria. J. Phys. Chem., 70, 2126-2130, 1996.

Stolaki, S., Haeffelin, M., Lac, C., Dupont, J. C., Elias, T., Masson, V.: Influence of aerosols on the life cycle of radiation fog event. A numerical and observational study. Atmospheric Research, 151, 145-161, 2015.

Terai, C. R., Bretherton, C. S., Wood, R., Painter, G.: Aircraft observations of aerosol, cloud, precipitation and boundary layer properties in pockets of open cells over the southeast Pacific. Atmos. Chem Phys., 14, 8071-8088, doi:10.5194/acp-14-8071-2014, 2014.

Vautard, R., Yiou, P., Van Oldenborgh, G. J.: Decline of fog, mist and haze in Europe over the past 30 years. Nat. Geosci., 2, 115-119, 2009.

Wang, H., Feingold, G., Wood, R., Kazil, J.: Modelling microphysical and meterological controls on precipitation and cloud cellular structures in Southeast Pacific stratocumulus. Atmos. Chem. Phys., 10, 6347-6362, doi:10.5194/acp-10-6347-2010, 2010.

Wang, S., Zheng, X., Jiang, Q.: Strongly sheared stratocumulus convection: an observationally based large-eddy simulation study. Atmos. Chem. Phys., 12, 5223-5235, doi:10.5194/acp-12-5223-2012, 2012.

Wood, R., Irons, S., Jonas, P. R.: How important is the spectral ripening effect in stratiform boundary layer clouds? Studies using simple trajectory analysis. J. Atmos. Sci., 59, 2681-2693, 2002.

Wood, R., Bretherton, C. S.: Boundary layer depth, entrainment, and decoupling in the cloud-capped subtropical and tropical marine boundary layer. J. Clim., 17, 3576-3588, 2004.

Wood, R. and Hartmann, D. L.: Spatial variability of liquid water path in marine low cloud: The importance of mesoscale cellular convection, J. Clim., 19, 1748-1764, 2006.

Wood, R., Leon, D., Lebsock, M., Snider, J., Clarke, A. D.: Precipitation driving of droplet concentration variability in marine low clouds. J. Geophys. Res., 117,D19210, doi:10.1029/2012JD018305, 2012.

Geosci. Model Dev. Discuss., doi:10.5194/gmd-2016-159, 2016
Manuscript under review for journal Geosci. Model Dev.
Published: 6 July 2016

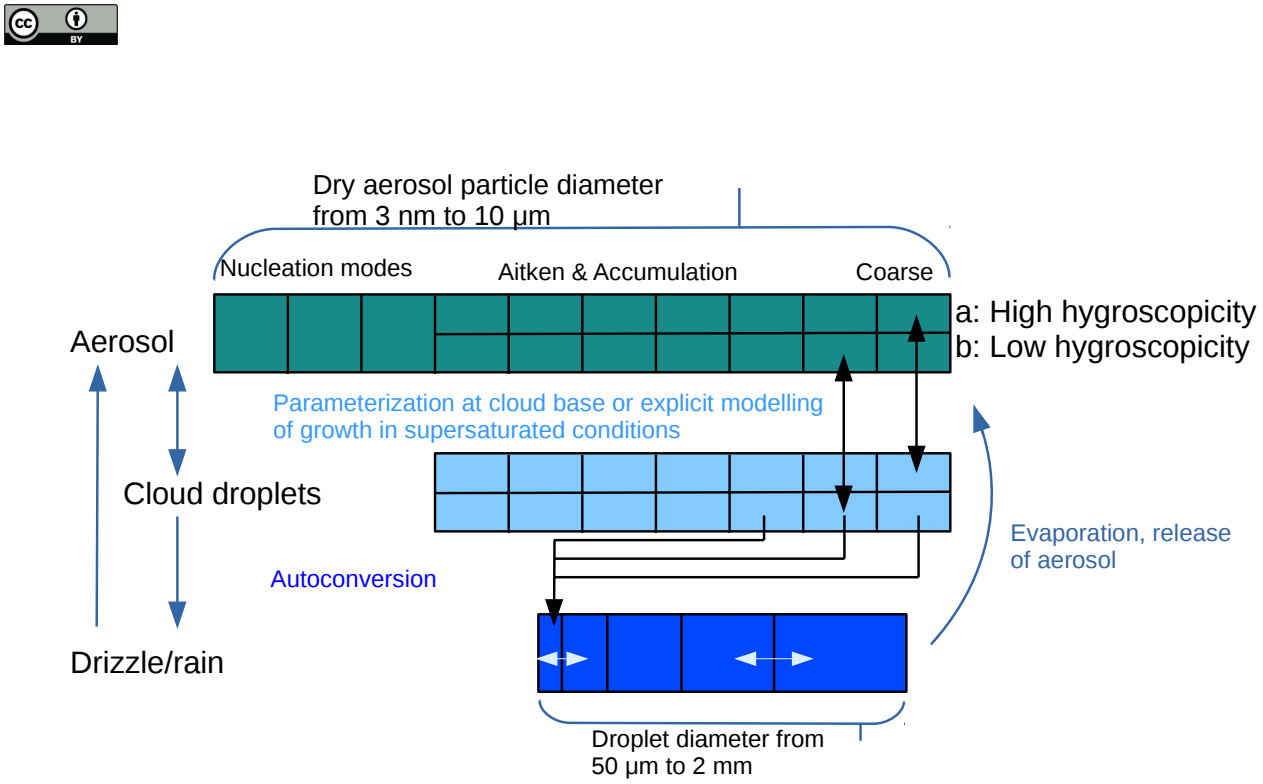

Figure 1. Schematic representation of the bin layout and processes included in the extended SALSA module. Aerosol and cloud droplet bins (green and light blue) are parallel with each other and follow the same size range for dry particle diameter (from 3 nm to 10 µm). In contrast, the drizzle bins (dark blue) are defined according to the wet diameter of the droplet and cover the size range between 50 µm and 2 mm.

Table 1. Model experiments with their key configuration details.

Experiment	SALSA	Particle number (cm^{-3})*
LEV3	off	55
LEV4	on	190
LEV3HI	off	165
LEV4HI	on	570

*This is the prescribed CCN concentrations when SALSA is not used, otherwise the total initial aerosol number concentration.

Yamaguchi, T., Feingold, G.: On the relationship between open cellular convective cloud patterns and the spatial distribution of precipitation. Atmos. Chem. Phys., 15, 1237-1251, doi:10.5194/acp-15-1237-2015, 2015.

Geosci. Model Dev. Discuss., doi:10.5194/gmd-2016-159, 2016
Manuscript under review for journal Geosci. Model Dev.
Published: 6 July 2016

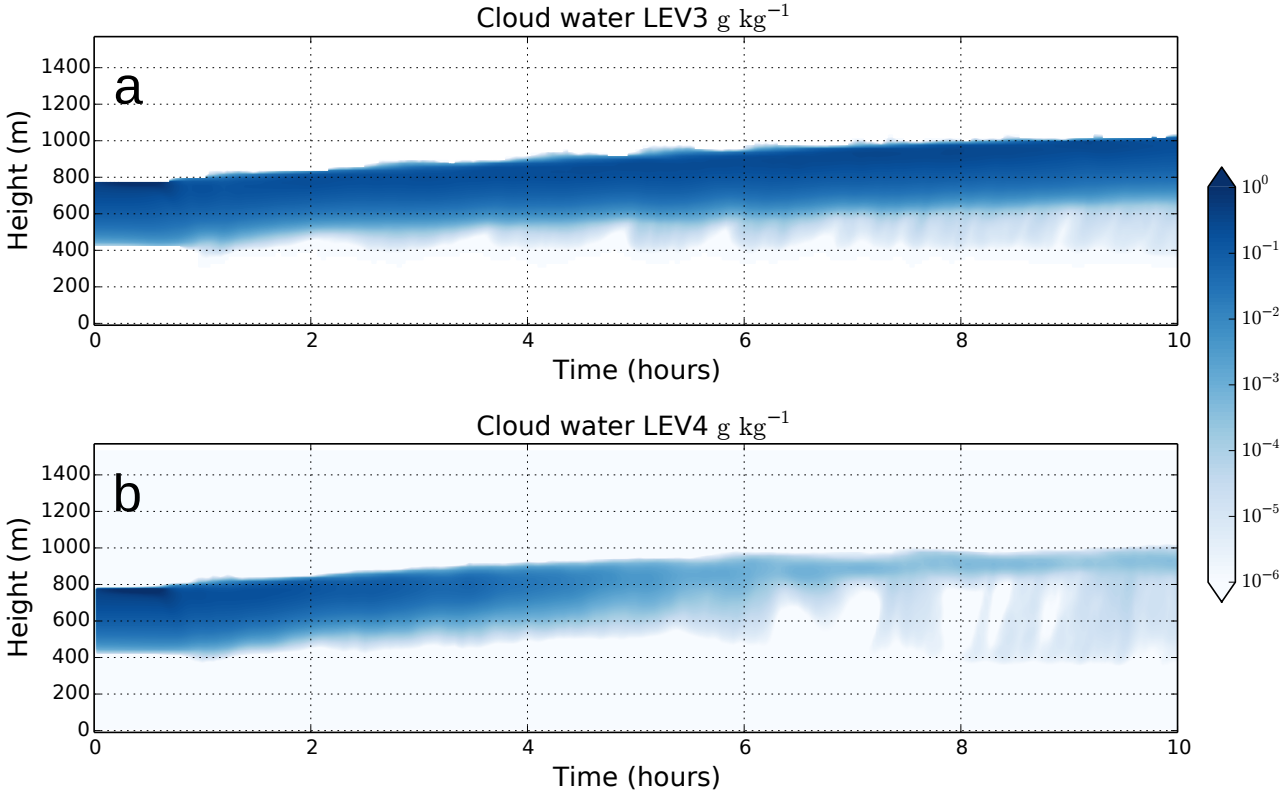

Figure 2. Time-height cross section of the cloud water content for LEV3 and LEV4 simulations in g kg^{-1}.

Geosci. Model Dev. Discuss., doi:10.5194/gmd-2016-159, 2016
Manuscript under review for journal Geosci. Model Dev.
Published: 6 July 2016

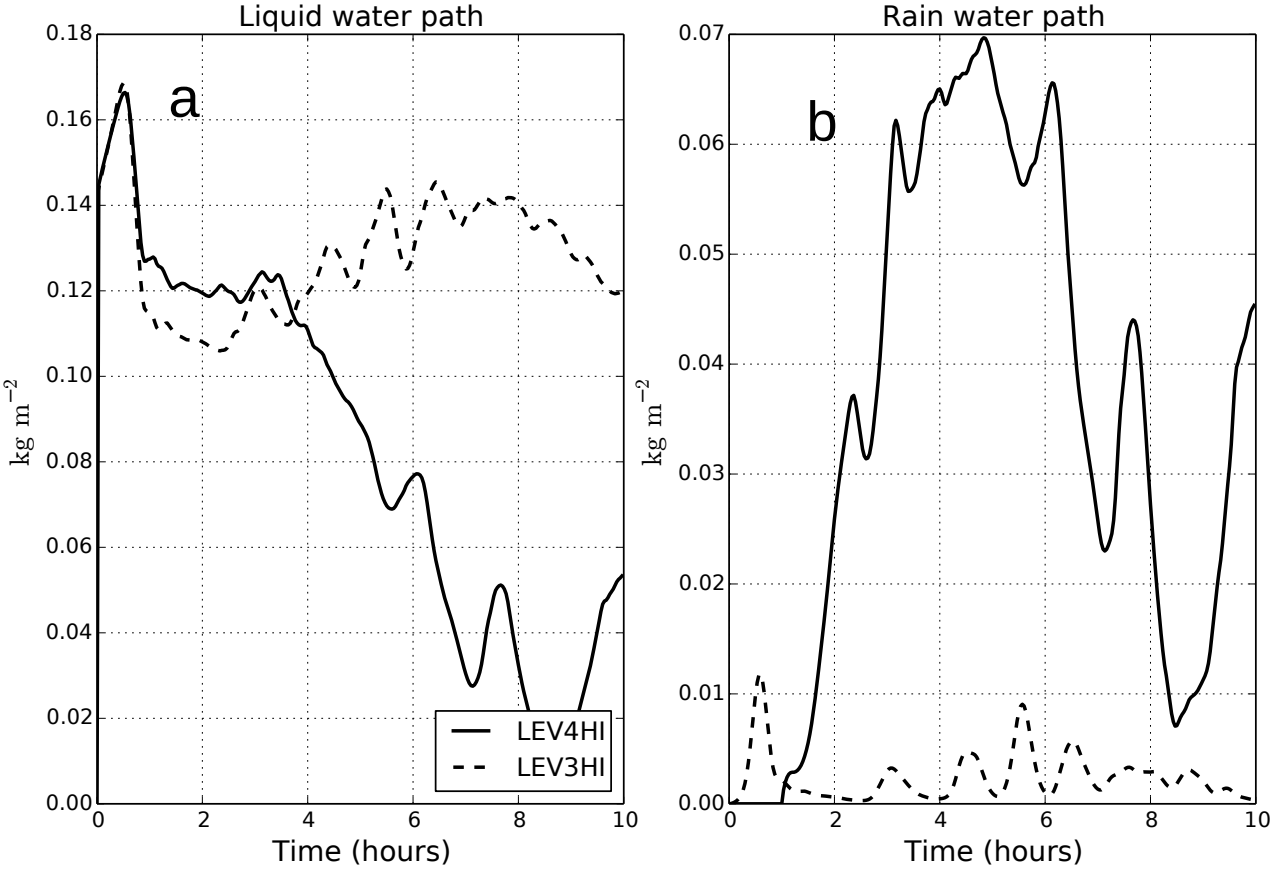

Figure 3. a) Liquid water path, interpreted as the total mass of water, including both cloud droplets and drizzle. b) Rain water path, taken as the water mass diagnosed in drizzle and rain drop bins only. Results from LEV3 are shown with a dashed line while those from LEV4 are shown with a solid line.

Geosci. Model Dev. Discuss., doi:10.5194/gmd-2016-159, 2016
Manuscript under review for journal Geosci. Model Dev.
Published: 6 July 2016

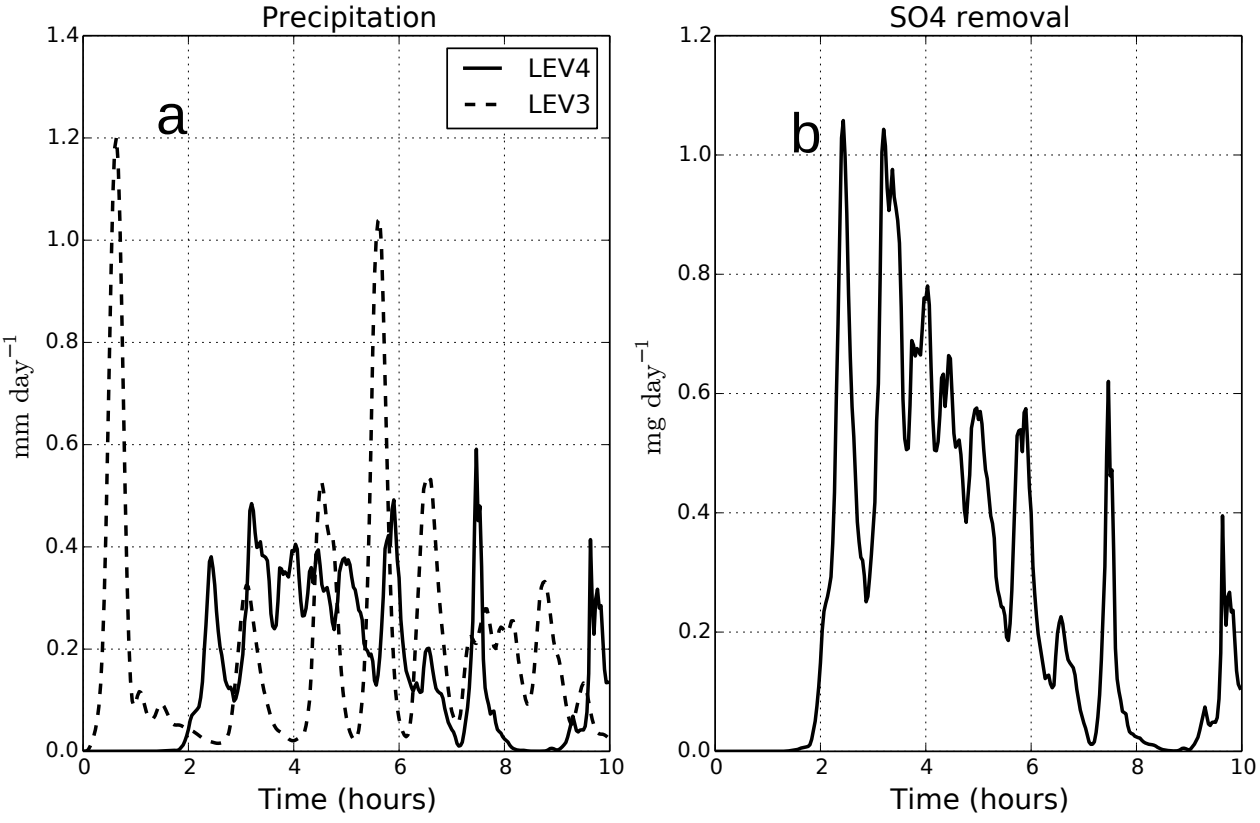

Figure 4. a) Surface precipitation rate in $\mathrm{mm\,day^{-1}}$ and b) removal rate of sulphate embedded in precipitating drops in $\mathrm{mg\,day^{-1}}$. Results from LEV3 are shown with a dashed line while those from LEV4 are shown with a solid line.

Geosci. Model Dev. Discuss., doi:10.5194/gmd-2016-159, 2016
Manuscript under review for journal Geosci. Model Dev.
Published: 6 July 2016

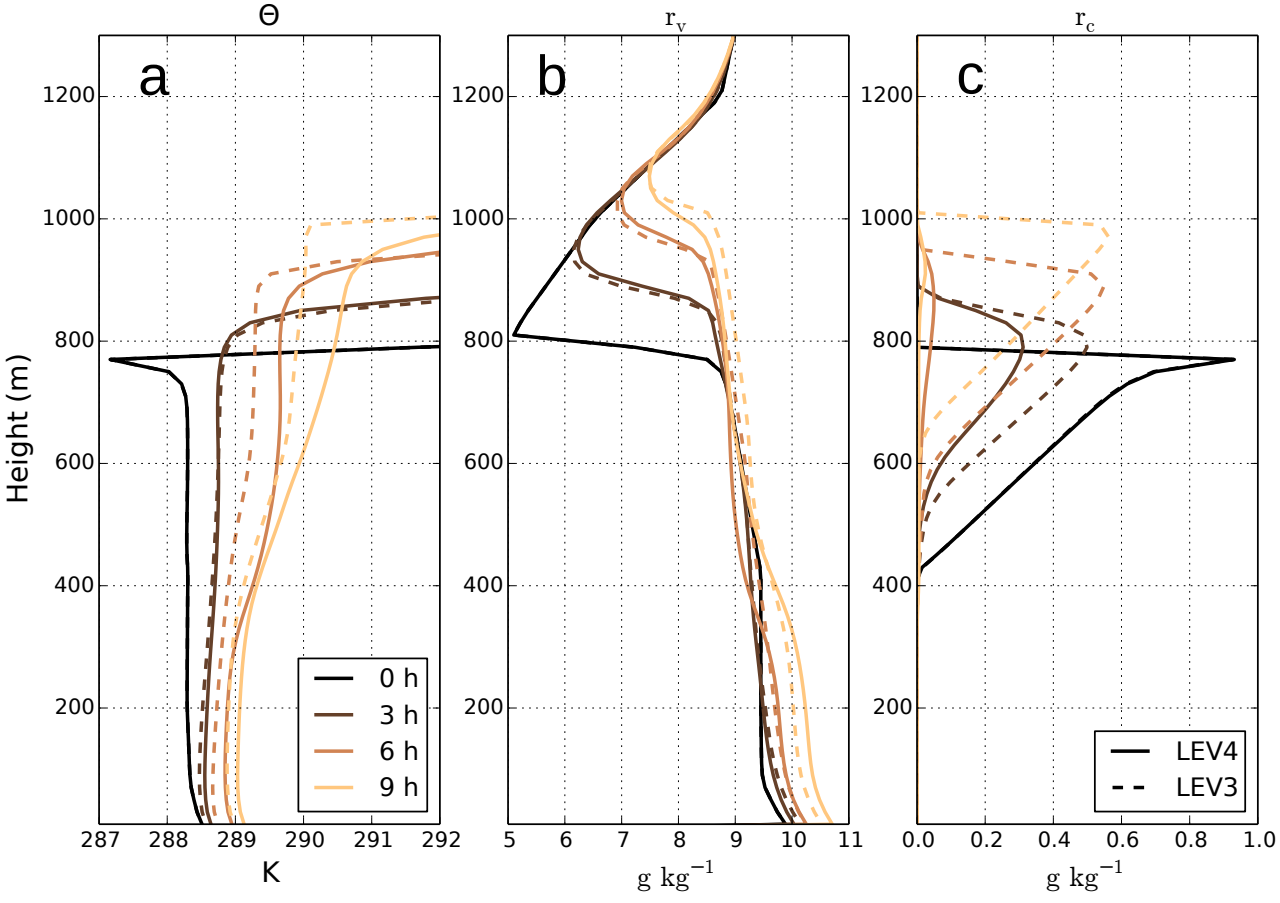

Figure 5. Domain mean vertical profiles of a) potential temperature, b) water vapour mixing ratio and c) liquid water mixing ratio. Data is plotted in 3 hour intervals from the initial state of the model to 9 hours into the simulation (from black to orange). Results from LEV3 are shown with a dashed line while those from LEV4 are shown with a solid line.

Geosci. Model Dev. Discuss., doi:10.5194/gmd-2016-159, 2016
Manuscript under review for journal Geosci. Model Dev.
Published: 6 July 2016

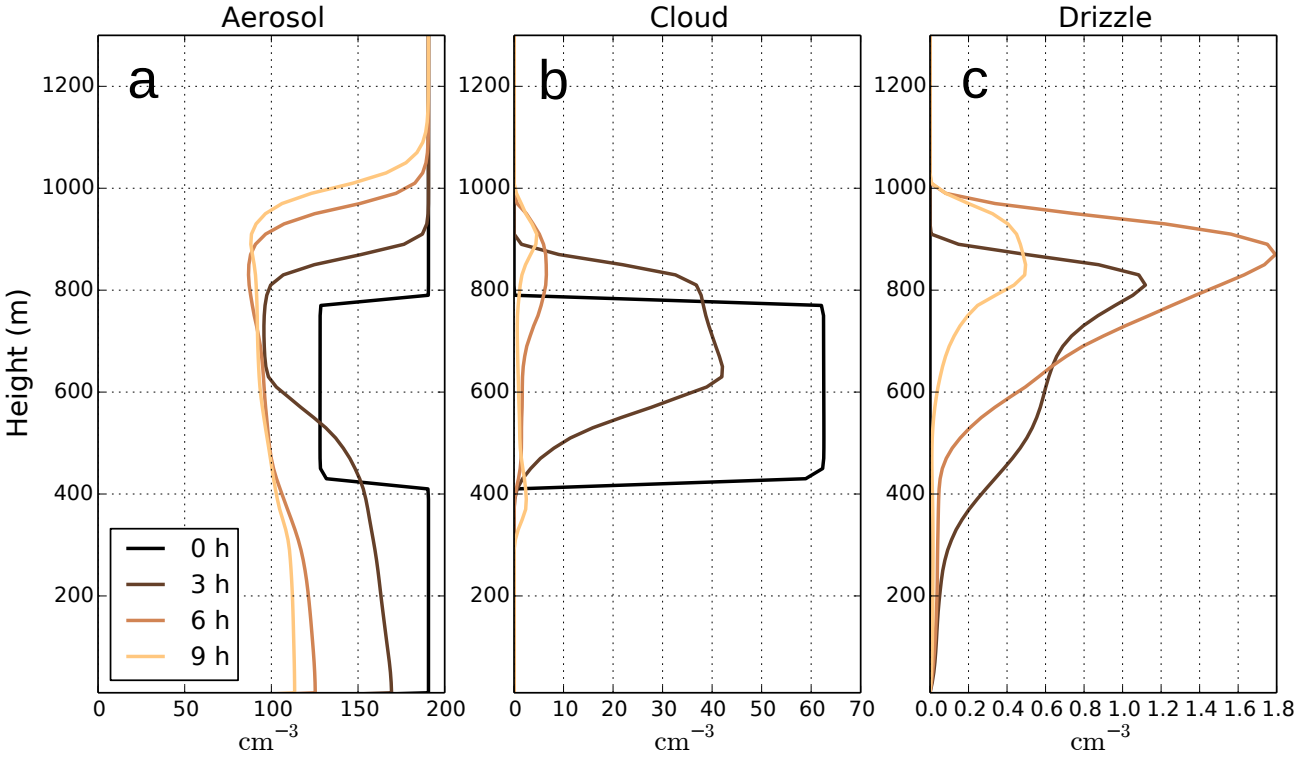

Figure 6. LEV4 domain mean profiles for a) aerosol, b) cloud droplet and c) drizzle number concentrations, plotted in 3 hour intervals from the initial state of the model to 9 hours into the simulation (from black to orange).

Geosci. Model Dev. Discuss., doi:10.5194/gmd-2016-159, 2016
Manuscript under review for journal Geosci. Model Dev.
Published: 6 July 2016

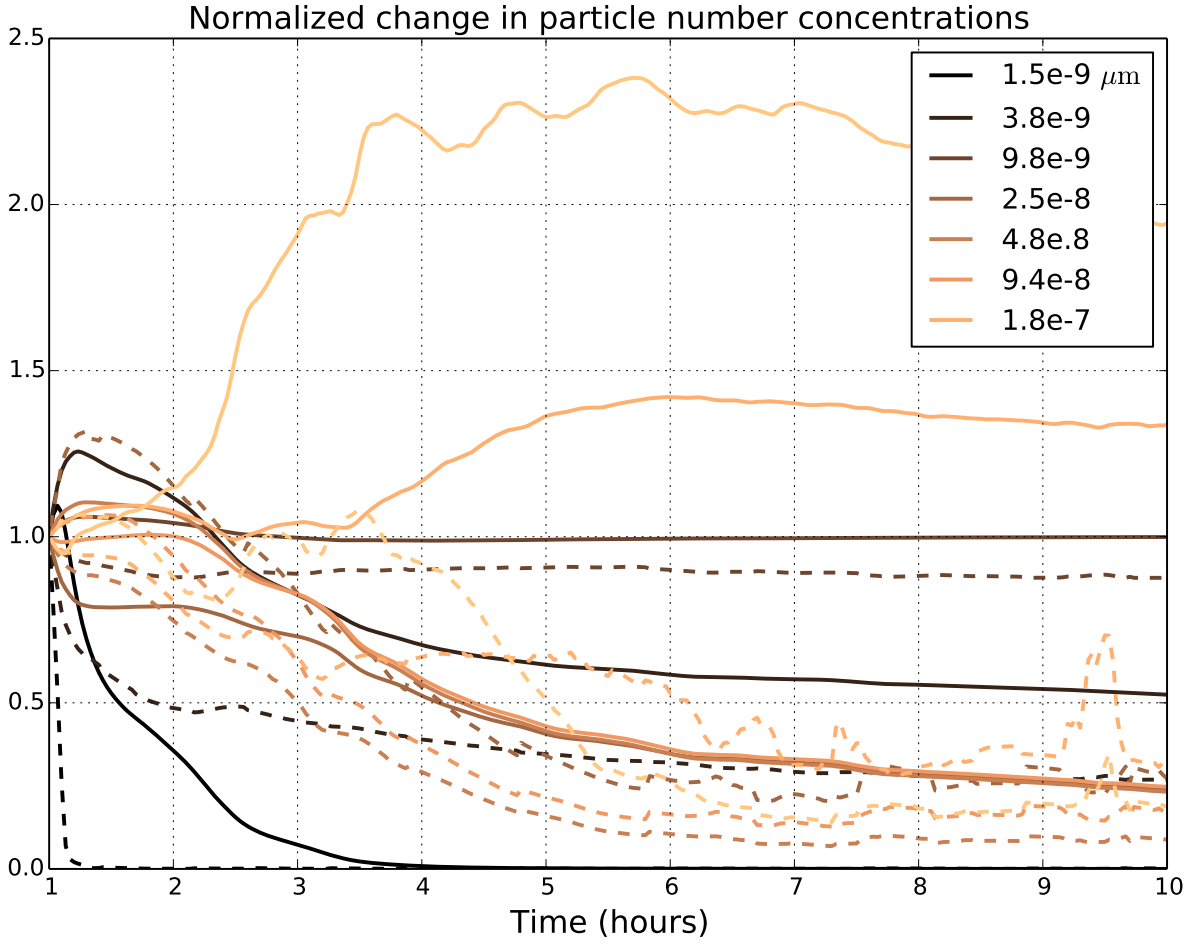

Figure 7. Normalized change in particle number concentration in each size bin. The concentrations are presented as a domain average from the i) below-cloud layer (solid lines) and ii) in-cloud (dashed lines). In the latter case, the sum of the number of interstitial particles and activated CCN is presented for each bin. The two largest size bins are not shown because of very small absolute concentrations in this case. The legend gives the lower limit diameter of the presented size bins. Data is show from the end of the spinup period. Number concentrations from this time are used as the normalizing factor for each bin.

Geosci. Model Dev. Discuss., doi:10.5194/gmd-2016-159, 2016
Manuscript under review for journal Geosci. Model Dev.
Published: 6 July 2016

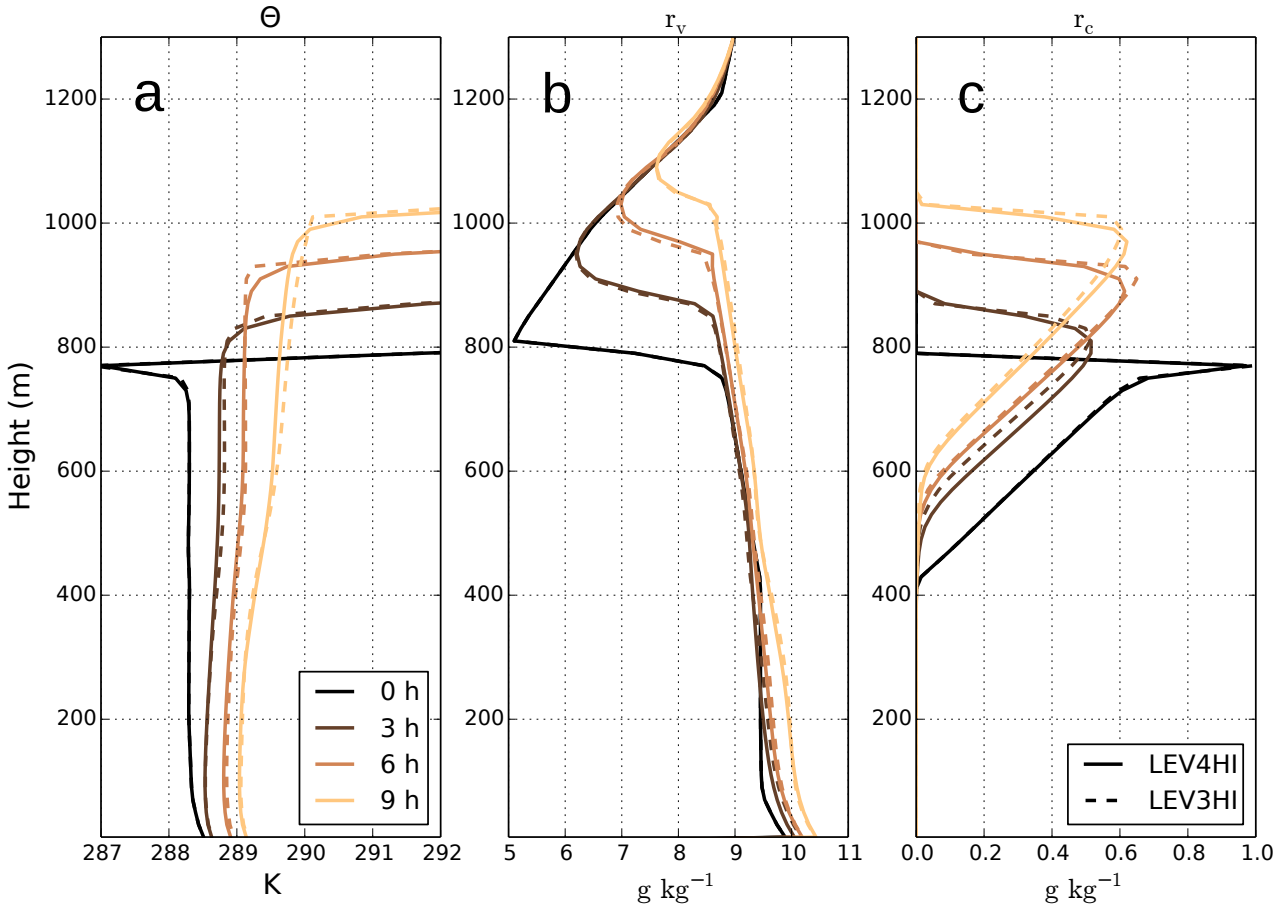

Figure 8. Similar to Figure 5, but for the experiments LEV3HI and LEV4HI with high aerosol number concentrations.

Geosci. Model Dev. Discuss., doi:10.5194/gmd-2016-159, 2016
Manuscript under review for journal Geosci. Model Dev.
Published: 6 July 2016

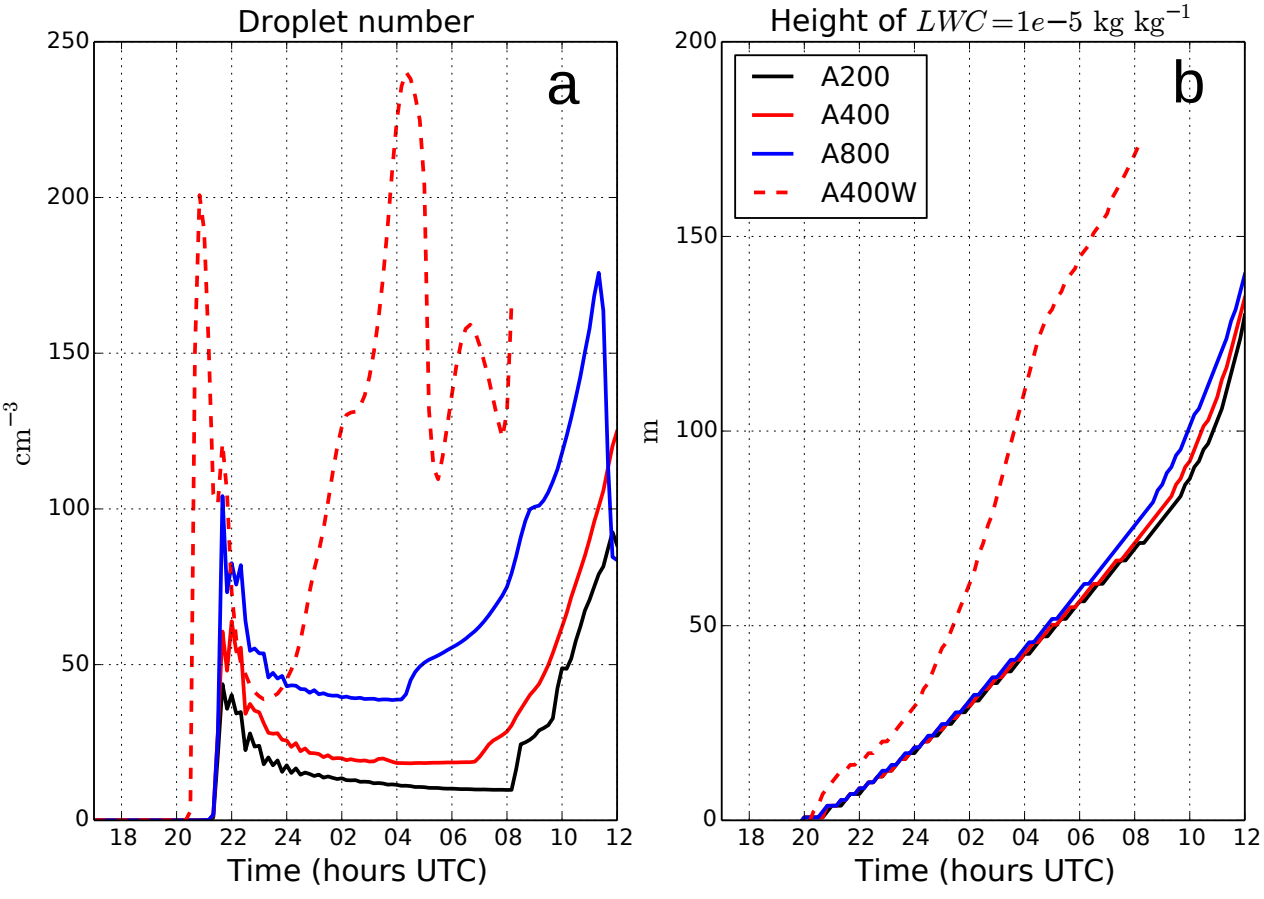

Figure 9. a) Fog droplet number concentrations and b) the height of the fog top layer interpreted as the 1×10^{-5} kg kg^{-1} isoline for liquid water mixing ratio.

Geosci. Model Dev. Discuss., doi:10.5194/gmd-2016-159, 2016
Manuscript under review for journal Geosci. Model Dev.
Published: 6 July 2016

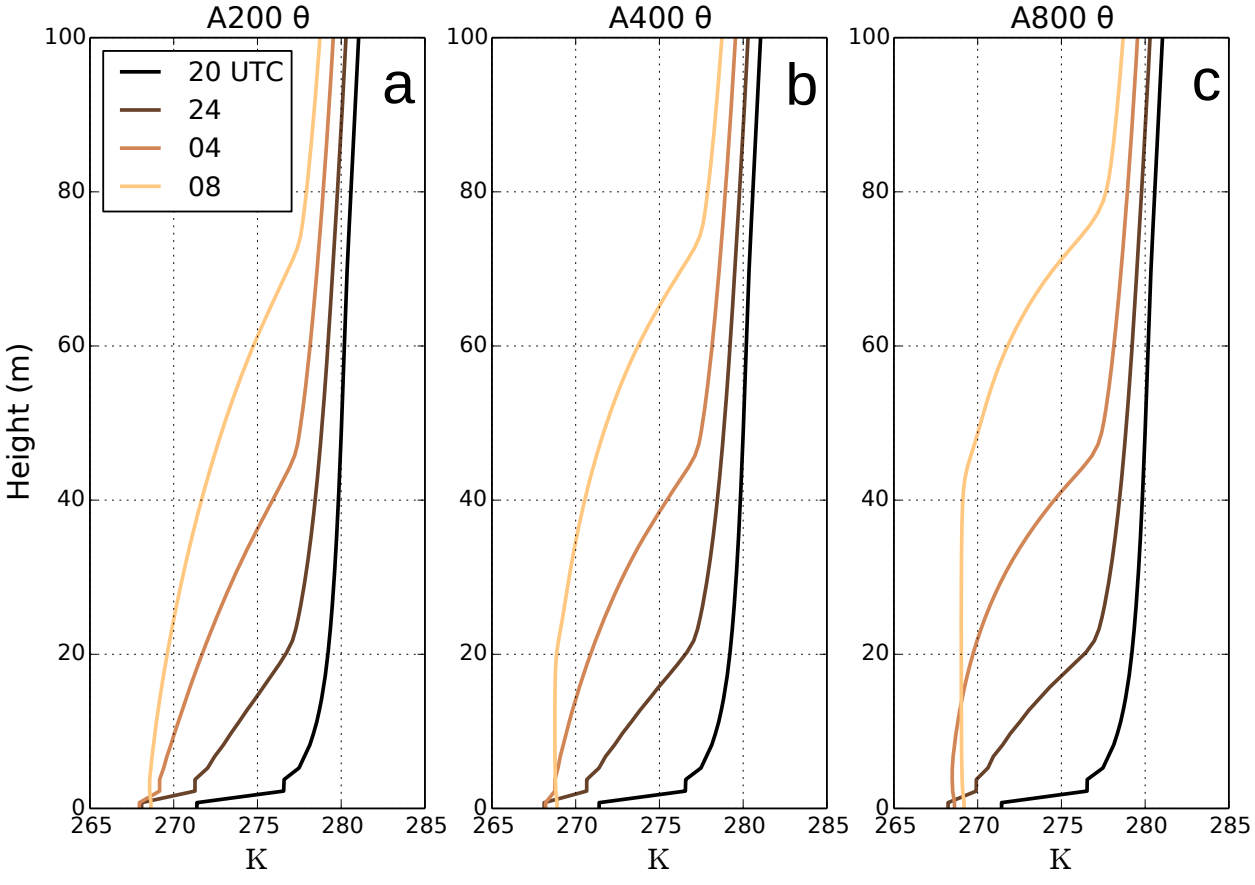

Figure 10. Domain mean profiles of potential temperature in 4 hour intervals starting from the formation of the fog layer (from black to orange) for the experiments a) A200, b) A400 and c) A800.

Geosci. Model Dev. Discuss., doi:10.5194/gmd-2016-159, 2016
Manuscript under review for journal Geosci. Model Dev.
Published: 6 July 2016

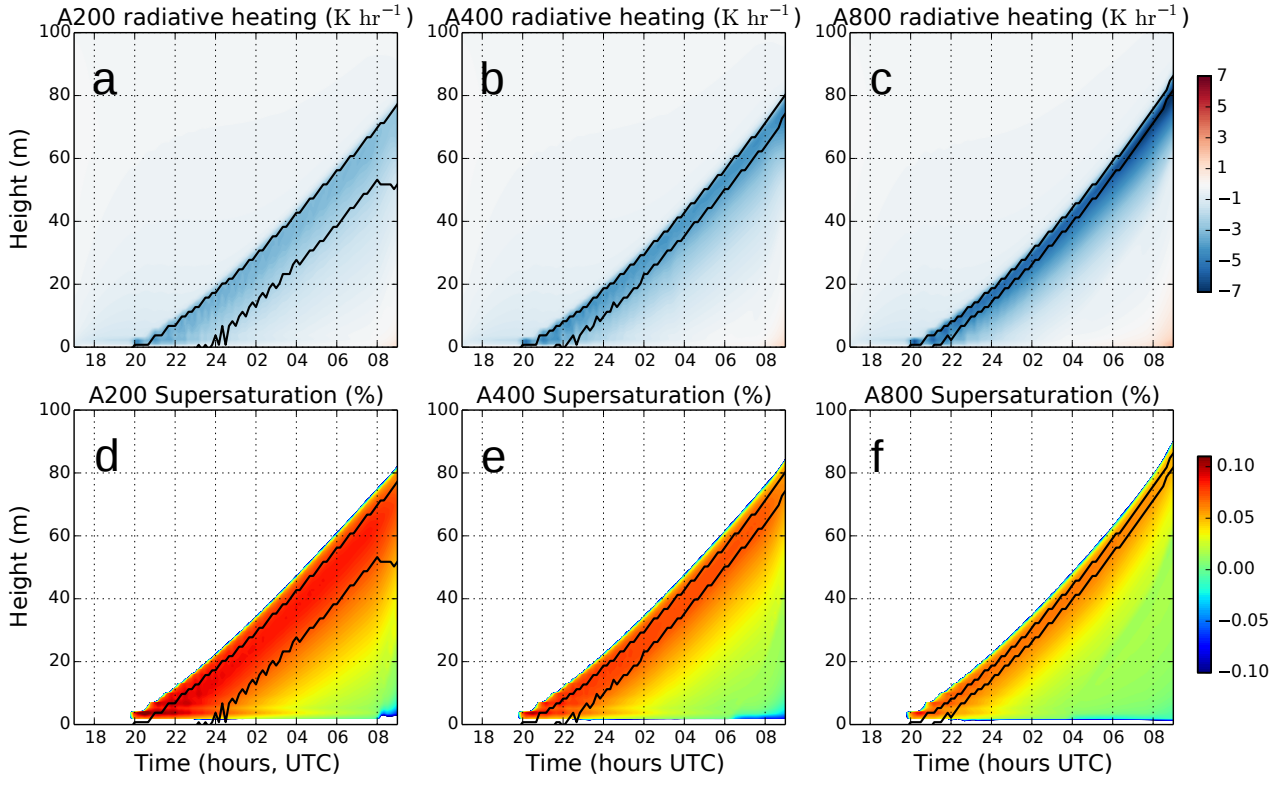

Figure 11. a)-c) Radiative heating in $\mathrm{K\,hr^{-1}}$ for the experiments A200,A400 and A800, respectively. d)-f) Water vapour supersaturation in per cent for the same experiments. The upper and lower black curves give the $0.01\ \mathrm{g\,kg^{-1}}$ and $0.1\ \mathrm{g\,kg^{-1}}$ isolines for the liquid water mixing ratio, respectively.

Geosci. Model Dev. Discuss., doi:10.5194/gmd-2016-159, 2016
Manuscript under review for journal Geosci. Model Dev.
Published: 6 July 2016

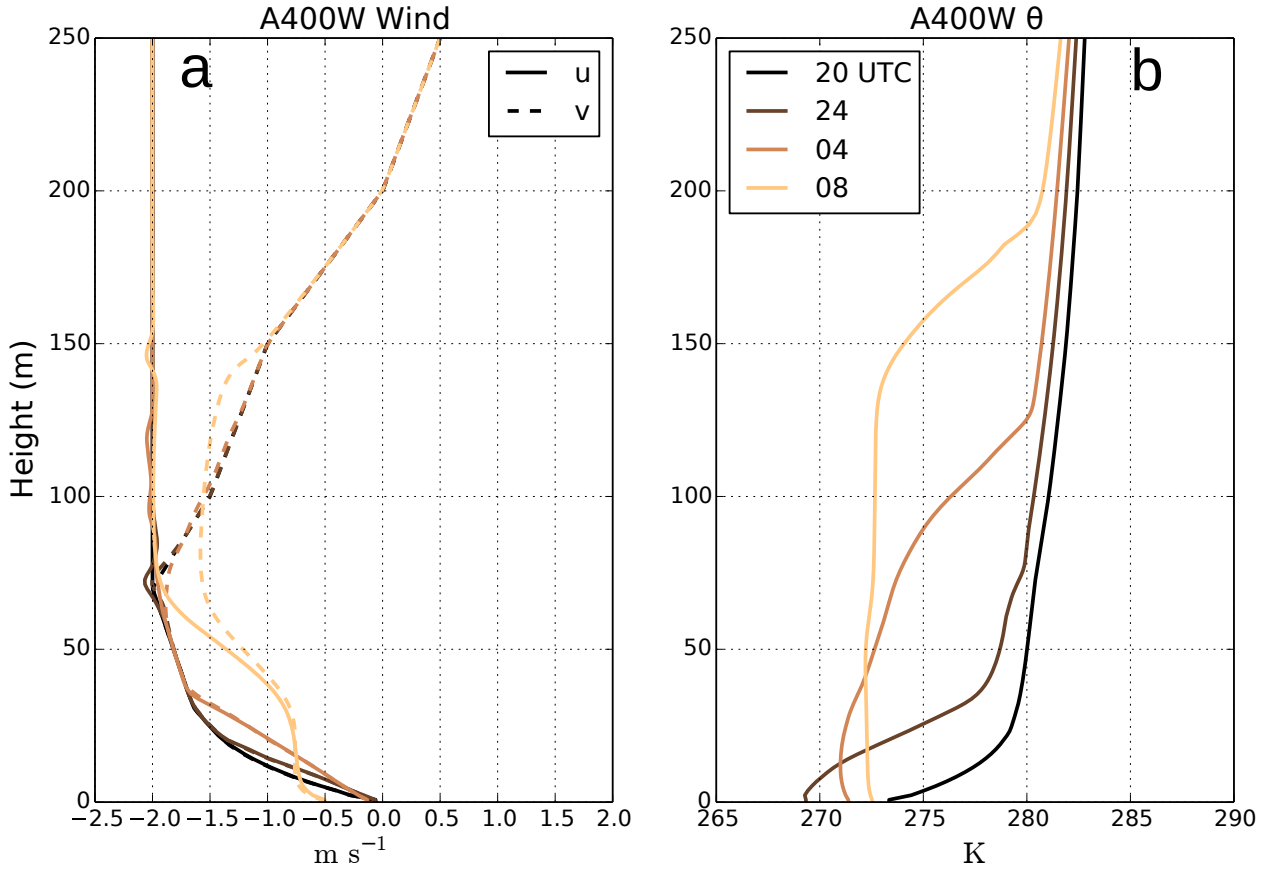

Figure 12. a) Domain mean profiles of u and v wind components and b) the potential temperature for the experiment A400W in 4 hour intervals from the formation of the fog layer (from black to orange).